DOI: 10.1016/j.ijpharm.2023.123348

Repositioning the antihistamine ebastine as an intracellular siRNA delivery enhancer

Authors: Cristina Muntean[1,2], Eva Blondeel[2,3], Laure Harinck[1], Kunal Pednekar[4], Jai Prakash[4], Olivier De Wever[2,3], Jeanne Leblond Chain[5], Stefaan C. De Smedt[1,6], Katrien Remaut[1], Koen Raemdonck[1,2]

Affiliations:

[1] Ghent Research Group on Nanomedicines, Laboratory of General Biochemistry and Physical Pharmacy, Faculty of Pharmaceutical Sciences, Ghent University, Ottergemsesteenweg 460, 9000 Ghent, Belgium

[2] Cancer Research Institute Ghent (CRIG), Ghent University, Ghent, Belgium

[3] Laboratory of Experimental Cancer Research, Department of Human Structure and Repair, Ghent University, UZ-Gent, 2RTP, Corneel Heymanslaan 10, 9000 Ghent, Belgium

[4] Engineered Therapeutics Group, Department of Advanced Organ Bioengineering and Therapeutics, Technical Medical Centre, University of Twente, 7500 AE Enschede, The Netherlands

[5] University of Bordeaux, CNRS, INSERM, ARNA, UMR 5320, U1212, F-33000 Bordeaux, France

[6] Ghent Light Microscopy (GLiM) Core, Ghent University, Ottergemsesteenweg 460, 9000 Ghent, Belgium

Abstract:

Small interfering RNAs (siRNAs) are promising therapeutics for the treatment of human diseases via the induction of sequence-specific gene silencing. To be functional, siRNAs require cytosolic delivery into target cells. However, state-of-the-art delivery systems mediate cellular entry through endocytosis and suffer from ineffective endosomal escape, routing a substantial fraction of the siRNA towards the lysosomal compartment. Cationic amphiphilic drugs (CADs) have been described to improve cytosolic siRNA delivery by the transient induction of lysosomal membrane permeabilization. In this work, we evaluated ebastine, an antihistamine CAD, for its ability to enhance cytosolic release of siRNA in a non-small cell lung cancer model. In particular, we demonstrate that ebastine can improve the siRNA-mediated gene silencing efficiency of a polymeric nanogel by 40-fold, outperforming other CAD compounds. Additionally, ebastine substantially enhanced gene knockdown of a cholesterol-conjugated siRNA, in two-dimensional (2D) cell culture as well as in three-dimensional (3D) tumor spheroids. Finally, ebastine could strongly promote siRNA delivery of lipid nanoparticles (LNPs) composed of a pH-dependent switchable ionizable lipid and with stable PEGylation, in contrast to state-of-the-art LNP formulations. Altogether, we identified ebastine as a potent and versatile siRNA delivery enhancer in cancer cells, which offers opportunities for drug combination therapy in oncology.

Graphical abstract

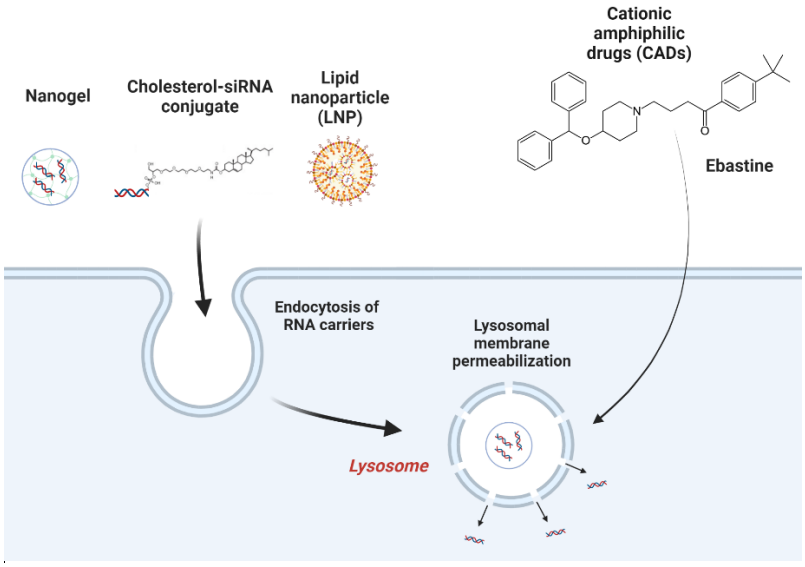

1. Introduction

Since its discovery more than two decades ago, RNA interference (RNAi) has developed into a powerful approach for sequence-specific gene silencing, holding great potential for biomedical applications.[1] In contrast to conventional small molecule drugs, RNAi effectors such as small interfering RNA (siRNA) can silence the expression of virtually any disease-causing gene, thereby greatly expanding the pool of 'druggable' targets.[2] However, therapeutic application requires extensive chemical modifications and/or encapsulation in a nanocarrier to protect the siRNA payload against degradation, modulate biodistribution and promote intracellular delivery.[3,4] To date, successful clinical translation has been demonstrated both with lipid nanoparticle (LNP) technology as well as bioconjugates (*e.g.* N-acetylgalactosamine (GalNAc) siRNA conjugates), both achieving efficient siRNA delivery to the liver.[5] The first siRNA-based therapeutic (Onpattro®, patisiran), *i.e.* an LNP formulation containing the ionizable lipid DLin-MC3-MDA, was approved by the FDA in 2018.[6] In the following years, also a number of GalNAc siRNA conjugates entered into the market (*i.e.* givosiran, lumasiran, vutrisiran, inclisiran), which rely on extensive chemical modification of the siRNA and high affinity binding of the triantennary GalNAc moiety to the highly abundant asialoglycoprotein receptor (ASGPR), expressed on hepatocytes.[7,8] Finally, for extrahepatic delivery, extensive studies were performed on the application of cholesterol-conjugated siRNAs, which demonstrated significant knockdown efficiency against cancer-associated targets in solid tumors, albeit requiring high doses. [7–12]

Despite significant advances in delivery of RNA-based therapeutics, specific extra- and intracellular barriers still represent a limiting factor for their clinical translation.[13,14] At the cellular level, both LNP-encapsulated siRNA as well as siRNA conjugates are internalized by target cells through the endocytic pathway after which they are trafficked towards the lysosomes and consequently degraded. Nevertheless, to be functional, siRNA requires release into the cytosol. [15] However, only 1-3% of LNP-formulated siRNA was shown to escape from the endosomal confinement, a number which is even substantially lower in the case of GalNAc-siRNAs (< 0.2%). [16–19] Improving cytosolic delivery of siRNA could thus be an important dose-sparing strategy. Our group recently reported on the repurposing of cationic amphiphilic drugs (CADs) as intracellular siRNA delivery enhancers.[20,21] Many CADs are well-known and

widely-used drugs, such as antihistamines, antidepressants and antihypertensives. Due to their physicochemical properties (pKa > 6 and logP > 3), CAD molecules can diffuse through cellular membranes and accumulate in acidic organelles, mostly lysosomes.[22] Here, CADs transiently induce an acquired phospholipidosis phenotype through functional inhibition of acid sphingomyelinase (ASM), a lysosomal enzyme that hydrolyzes sphingomyelin to ceramide.[23] It was demonstrated that this lysosomal phenotype coincides with lysosomal swelling and the temporary induction of lysosomal membrane permeabilization (LMP), allowing siRNA molecules to escape from the lysosome into the cytosol.[20,21]

Based on this mechanism, CADs are also being investigated in cancer therapy.[24] Lysosomotropic CADs can selectively induce caspase 3-independent lysosomal cell death (LCD) through lysosomal destabilization, allowing treatment of apoptosis-resistant cancer types.[25–28] Of note, it is proposed that tumors are more sensitive to CAD-induced lysosomal damage than healthy tissues.[29] Within the group of CADs, antihistamines are of particular interest, in part because of their wide use, good tolerability and low cost.[30,31] More specifically, the antihistamine ebastine has demonstrated cytotoxic effects on various cancer cell models, which makes it an interesting CAD in the context of tumor treatment.[30,32–34] On the other hand, it is thought that the provoked LMP alone will not suffice in cancer therapy.[35,36] Many LMP-inducing CADs, including antihistamines, are prescribed to millions of patients globally, but pharmacological tissue drug levels are likely too low to induce potent LCD in anti-cancer monotherapy. Therefore, combination treatment with other drugs is required to support clinical translation of CADs as anti-cancer drugs. For example, antihistamines have been combined with conventional chemotherapy or with immune checkpoint blocking (ICB) antibodies to improve therapeutic response.[30,37,38]

The recent discovery that CADs can promote intracellular siRNA delivery could provide additional opportunities for drug combination therapy. Ebastine is recognized as a potent LCD inducer, but its value as siRNA delivery enhancer was not yet explored.[20,30] Based on the specific potential of antihistamine repurposing in cancer therapy, in this study we therefore explored the effect of the antihistamine ebastine on improving the siRNA silencing efficiency of selected nanocarriers, including a polymeric hydrogel nanocarrier, cholesterol-conjugated siRNA and state-of-the-art LNP formulations, in a non-small cell lung cancer (NSCLC) cell

model. We initially compared the adjuvant effect of ebastine with two other model CAD drugs, namely desloratadine and lofepramine. The tricyclic antihistamine desloratadine was previously identified as one of the most promising CAD molecules for siRNA adjuvant therapy.[21] Lofepramine is a tricyclic antidepressant that was discovered as a siRNA delivery potentiator through screening of the NIH Clinical Compound Collection.[21] It is demonstrated that ebastine strongly promotes siRNA silencing efficiency for all delivery systems tested. In case of LNPs, the ebastine adjuvant effect was highly dependent on the LNP composition and PEGylation strategy. Finally, improved target gene knockdown following ebastine-induced siRNA release could be established for cholesterol-siRNA conjugates in a 3D tumor spheroid model.

2. Materials and Methods

2.1 Small interfering RNAs (siRNAs)

The 21-nucleotide siRNA duplexes targeting the enhanced green fluorescent protein (siEGFP) and the negative control siRNA (siCTRL) were purchased from Eurogentec (Seraing, Belgium). The siCTRL sequence presents no homology with any known eukaryotic gene. Sequences of siEGFP: sense strand = 5'-CAAGCUGACCCUGAAGUUCtt-3'; antisense strand = 5'-GAACUUCAGGGUCAGCUUGtt-3'. Sequence of siCTRL: sense strand = 5'-UGCGCUACG-AUCGACGAUGtt-3'; antisense strand = 5'- CAUCGUCGAUCGUAGCGCAtt-3'. Capital letters represent ribonucleotides, lower case letters represent 2'-deoxyribonucleotides. Cholesterol-conjugated Accell siRNAs (Dharmacon, Lafayette, CO, USA) have the following antisense sequences: (Cy3-labeled) non-targeting = UGGUUUACAUGUCGACUAA; eGFP targeting = GCCACAACGUCUAUAUCAU. The siRNA was dissolved in nuclease-free water (Ambion-Life Technologies, Ghent, Belgium) and stored at -80°C. The concentration of the siRNA stock was calculated by UV spectrophotometry at 260 nm (1 OD_{260} = 40 µg/mL) with a NanoDrop 2000c UV−Vis spectrophotometer (Thermo Fisher Scientific, MA, USA).

2.2 Cell line and culture conditions

Human non-small cell lung cancer (NSCLC) cell lines that stably express eGFP are applied (A549-eGFP and H1299-eGFP). H1299-eGFP was kindly provided by the lab of Prof. Camilla Foged (Department of Pharmacy, University of Copenhagen, Copenhagen, Denmark). The

A549-eGFP cell line was kindly provided by the lab of Prof. Olivier de Wever (Faculty of Medicine and Health Sciences, University of Ghent, Ghent, Belgium).[39] H1299-eGFP cells were cultured in Roswell Park Memorial Institute (RPMI) 1640 medium (Gibco®-Life Technologies, Grand Island, NY, USA) and A549-eGFP cells in Dulbecco's Modified Eagle Medium (DMEM) with high glucose content (Gibco®-Life Technologies, Grand Island, NY, USA), both supplemented with 10% fetal bovine serum (FBS, Hyclone™, GE Healthcare, Machelen, Belgium), 2 mM L-Glutamine and 100 U/mL penicillin/streptomycin (*i.e.* complete cell culture medium or CCM). The cell lines were maintained in a humidified atmosphere containing 5% CO_2 at 37°C and culture medium was renewed every other day. When 80-90% confluence level was reached, cells were split using 0.25% trypsin-ethylenediaminetetraacetic acid (EDTA). Cells were regularly tested and found negative for mycoplasma. To produce spheroids, U-bottom 96-well ULA plates (cat. no. MS-9096UZ, S-bio) were seeded with a suspension of 100 µl of A549-eGFP cells with 4000 cells/well in 3 technical replicates per condition. The spheroids were allowed to grow for 3 days at 37°C and 5% CO_2.

2.3 Preparation of siRNA-loaded cationic dextran nanogels

Dextran hydroxyethyl methacrylate (dex-HEMA) nanogels were prepared with a degree of substitution of 5.2 by an inverse miniemulsion photopolymerization method as reported previously.[40–43] Briefly, dex-HEMA was copolymerized with a cationic methacrylate monomer (2-(methacryloyloxy)ethyl trimethylammonium chloride (TMAEMA)) to form cationic dex-HEMA-*co*-TMAEMA nanogels (dex-HEMA NGs). The obtained nanogels were lyophilized and stored desiccated to ensure long term stability. A NG stock of 2 mg/mL was prepared by dispersing a weighed amount of lyophilized particles in ice-cooled nuclease-free water, followed by brief sonication (3 x 5 s, amplitude 10%; Branson Digital Sonifier®, Danbury, USA). This method leads to nanogels with a diameter of about 200 nm and a ζ-potential of about 25 mV, in line with earlier reports in the literature.[44] Before transfection, equal volumes of siRNA and NGs in 4-(2-hydroxyethyl)-1-piperazineethanesulfonic acid (HEPES) buffer (20 mM, pH 7.4) were mixed and incubated at 4°C for 10 min to allow electrostatic complexation. The concentration of siRNA dilutions used for NG loading was adjusted to obtain a final cell concentration in the range of 0.05-250 nM (corresponding to 0.00167 - 8.3 pmol siRNA/µg NG). After a 5x dilution in Opti-MEM (Invitrogen, Merelbeke, Belgium), siRNA-loaded NGs were applied on cells at a fixed NG concentration of 30 µg/ml.

2.4 Preparation of siRNA-encapsulated lipid nanoparticles (LNPs)

DLin-MC3-DMA was purchased from MedChem Express (Bio-Connect, Huissen, The Netherlands). CSL3 lipid was kindly provided by Jeanne Leblond Chain (French Institute of Health and Medical Research, Bordeaux, France).[45] All other lipids were purchased from Avanti Polar Lipids, Inc. (Alabaster, AL, USA). LNPs were formulated through microfluidic mixing with varying lipid composition: (1) DLin-MC3-DMA:Cholesterol:DSPC:DSPE-PEG_{2000} at molar ratios of 50:38.5:10:1.5; (2) DLin-MC3-DMA:Cholesterol:DSPC:DMG-PEG_{2000} at molar ratios of 50:38.5:10:1.5; (3) CSL3:Cholesterol:DSPC:DSPE-PEG_{2000} at molar ratios 50:37.5:10:2.5; (4) CSL3:Cholesterol:DSPC:DMG-PEG_{2000} at molar ratios 50:37.5:10:1.5. Lipids were dissolved in ethanol in a final volume of 16 µl while siRNA was dissolved in sodium acetate (NaOAc) buffer (50 mM, pH 4) in a final volume of 32 µl to obtain a nitrogen-to-phosphate (N:P) ratio of 4.7. Both phases were mixed in a cartridge of the microfluidic NanoAssemblr® Spark™ device (Precision NanoSystems Inc., Canada) and ejected into 48 µL of $PBS^{-/-}$ (without calcium, magnesium) at pH 7.4. Standard settings and operation volumes were used to formulate the LNPs, as recommended by the Spark™ user guide. Particles were stored at 4°C for a maximum of 2 weeks. RNA encapsulation efficiency was quantified by the Quant-iT™ RiboGreen™ RNA Assay Kit (Invitrogen, Merelbeke, Belgium) according to manufacturer's instructions. Hydrodynamic diameter and polydispersity index (PDI) was measured at 1/50 dilution in HEPES buffer (20 mM, pH 7.4) via Dynamic Light Scattering (DLS) at 25°C (Zetasizer Nano, Malvern Instruments Ltd., Worcestershire, UK).

2.5 Cell transfection with nanocarriers and sequential CAD exposure

H1299-eGFP cells were seeded at a cell density of 8000 cells/well in 96-well plates (Bioswisstec, Schaffhausen, Switzerland) and were allowed to settle overnight. The next day, siRNA-NG complexes were prepared as described above with siRNA concentrations ranging from 0.05-250 nM and diluted 5-fold in Opti-MEM before being applied on cells for 4 h. On the other hand, for transfections with LNPs, the carrier was diluted in CCM and applied on cells for 24 h. Next, transfection medium was removed and cells were washed with $PBS^{-/-}$ and incubated for 20 h with lofepramine 30 µM (Sanbio, Uden, Netherlands), desloratadine 30 µM (Sigma-Aldrich, Overijse, Belgium) and ebastine 15 µM (Sanbio, Uden, Netherlands). Following 24 h incubation in CCM at 37°C, lysosomes were labeled by incubation with 50 µL 75 nM

Lysotracker Deep Red (LDR) stain (Thermo Fisher Scientific, Waltham, MA, USA) in CCM for 30 min at 37°C. Expression of eGFP and LDR staining was detected via flow cytometry, using a CytoFLEX flow cytometer plate reader for 96-well plates (Beckman Coulter, Krefeld, Germany) and CytExpert software. Data analysis was performed using the FlowJo analysis software (Treestar, Costa Mesa, CA, USA) and the percentage of eGFP expression for each sample was calculated by normalizing the fluorescence signal of cells treated with siEGFP to the fluorescence of cells treated with siCTRL.

2.6 Cell transfection with cholesterol-conjugated siRNA

H1299-eGFP and A549-eGFP cells were seeded at a cell density of respectively 8000 and 10000 cells/well in 96-well plates (Bioswisstec, Schaffhausen, Switzerland) and were allowed to settle overnight. The next day, cells were transfected for 6 h with Accell chol-siRNA diluted in Opti-MEM at concentrations of 50-500 nM. After removing the transfection medium, cells were washed with $PBS^{-/-}$ and treated with ebastine (15 µM) in CCM for 20 h. Following an additional incubation in CCM for 24 h, samples were stained with LDR and prepared for flow cytometry detection as previously described. For each sample, side scatter (SSC) and LDR signal was normalized to non-treated cells and represented as mean fold change ± standard error of the mean (SEM). For uptake detection of chol-siRNA, a Cy3-labeled construct was applied on cells at concentrations of 50-500 nM and flow cytometry was performed after 6 h of transfection.

2.7 Cell viability assay

Cell viability on monolayered culture was measured via detection of cellular metabolic activity using a CellTiter-Glo® assay (Promega, Belgium). After siRNA-NG transfection and CAD treatment, the assay was performed following manufacturer's instructions. For spheroids, the cell viability was detected by microscopy imaging of visual alterations in the spheroid integrity and by performing CellTiter-Glo® 3D Cell Viability Assay (Promega, Belgium) according to the manufacturer's protocol after 20 h treatment with 5, 25, 50 µM of ebastine. Data are presented as percentage of viable cells calculated from the luminescence signal of each condition relatively to non-treated cells and by taking in account the background luminescence of the medium. Transmission images of spheroids were detected by a laser scanning confocal microscope (Nikon A1R HD confocal, Nikon, Japan), equipped with a 10× air objective lens (10× Plan Apo, NA 0.45, WD 4000µm, Nikon, Japan).

2.8 Cell uptake of Cy3-labeled Accell siRNA in 3D tumor spheroids

After growing for 3 days, the formed spheroids were washed twice with Opti-MEM and treated with Cy3-labeled Accell siRNA for 24 h in Opti-MEM at a final concentration of 1 µM. Microscopic imaging was performed after transferring the spheroids to a glass-bottom 96-well plate (Grainer Bio-one, Frickenhausen, Germany) to detect penetration of Cy3 signal by a laser scanning confocal microscope (Nikon A1R HD confocal, Nikon, Japan), equipped with a 10× air objective lens (10× Plan Apo, NA 0.45, WD 4000µm, Nikon, Japan) with a laser box (LU-N4 LASER UNIT 405/488/561/640, Nikon Benelux, Brussels Belgium) and detector box (A1-DUG-2 GaAsP Multi Detector Unit, GaAsp PMT for 488 and 561 and Multi-Alkali PMT for 640 and 405 nm). The 488 nm and 561 nm lasers were applied to excite the eGFP protein and the Cy3-labeled chol-siRNA respectively. Fluorescence emission was detected through 525/50 nm (MHE57030) and 595/50 nm (MHE57050) filter cubes, respectively. A Galvano scanner was used for unidirectional scanning to acquire the channels sequential with 2 times line averaging, a dwell time of 6.2 µs and scan speed of 0.031 FPS. The pinhole was set to 2.6 µm and the pixel size was 1.23 µm/pixel. NIS Elements software (Nikon, Japan) was applied for imaging. Images were analyzed with Fiji software.[46] Z-stacks were acquired with a step of 25 µm until a total depth of 75 µm for at least 3 spheroids. The reported images were detected at the depth of 50 µm. After imaging, spheroids were prepared for flow cytometry detection by removing the CCM, washing with $PBS^{-/-}$ and dissociating the cells with 0.25% trypsin-EDTA for 10 min. Following neutralization with 120 µL CCM, cell suspension was transferred to a U-bottom 96-well plate (Greiner Bio-One GmbH, Vilvoorde, Belgium) and centrifuged for 5 min at 400 g. The supernatant was then removed and the cells were resuspended in flow buffer. Data is presented as mean ± SEM of three independent spheroids.

2.9 Assessment of eGFP silencing in 3D tumor spheroids

Tumor spheroids were seeded and allowed to grow for 3 days. After two consecutive washing steps with Opti-MEM, chol-siRNA was applied in Opti-MEM at the final concentration of 400 nM and cells were incubated at 37°C for 24 h. Subsequently, spheroids were washed with CCM, ebastine (35 µM) in CCM was applied for 20 h followed by 24 h incubation in fresh CCM. For confocal imaging, spheroids were transferred to a glass-bottom 96-well plate (Grainer Bio-one, Frickenhausen, Germany), and stained with Hoechst 33342 for 1 h (Molecular Probes, Erembodegem, Belgium). Imaging was performed with a laser scanning confocal microscope

(Nikon A1R HD confocal, Nikon, Japan), equipped with a 10× air objective lens (10× Plan Apo, NA 0.45, WD 4000 µm, Nikon, Japan). The 409 nm and 488 nm lasers were applied to excite the DAPI labeled nuclei and the eGFP protein respectively. Fluorescence emission was detected through 450/50 nm (MHE57010) and 525/50 nm (MHE57030) filter cubes, respectively. Next, spheroids were prepared for flow cytometric detection as previously described and eGFP silencing data is presented as mean ± SEM of three independent spheroids.

2.10 Statistical analysis

Experiments were performed as technical triplicates with 3 independent biological repeats (n=3) and presented as mean ± standard error of the mean (SEM), unless otherwise stated. Statistical analysis was performed using the 8th version of the GraphPad Prism software. The IC_{50} curves were obtained by interpolating the data into a logarithmic non-linear fit dose-response curve. One-way ANOVA with Tukey Correction was applied to compare multiple conditions, whereas the student t-test was used for direct comparison of 2 conditions. A p value ≤ 0.05 was considered a priori to be statistically significant (ns $p > 0.05$, * $p \leq 0.05$, ** $p \leq 0.01$, *** $p \leq 0.001$, **** $p \leq 0.0001$).

3. Results and discussion

3.1 Adjuvant effect of ebastine on siRNA delivery mediated by polymeric nanogels

Previous work has demonstrated that sequential exposure of cationic dextran nanogel (NG)-transfected NSCLC cells (H1299-eGFP) to CADs could substantially improve siRNA delivery (Figure 1a).[20,21] Here, the impact of the antihistamine ebastine on siRNA delivery via NGs was compared with two other well-described CADs, *i.e.* desloratadine and lofepramine (Figure 1b). In line with earlier observations, desloratadine was less cytotoxic relative to the other CADs tested, while ebastine and lofepramine had similar toxicity profiles (Figure 1c).[20] For subsequent transfection experiments, a concentration was selected where ebastine (15 µM) and desloratadine (30 µM) show comparable toxicity (~30%). The adjuvant effect of lofepramine was tested at the same concentration as desloratadine (30 µM), for which substantially higher toxicity was noted (~60%). Transfection results clearly demonstrated that

ebastine outperforms the other two CAD molecules by inducing a 40-fold improvement in siRNA-induced gene silencing, reaching a half-maximal inhibitory concentration (IC_{50}) in the low picomolar range (Figure 1d, f). Here, silencing efficiency does not seem to correlate with cytotoxicity, as the highest toxicity was observed for the least performing CAD (*i.e.* lofepramine, 7-fold improvement in gene silencing). It was previously reported by du Rietz *et al*. that different CAD molecules can target distinct endocytic compartments (*e.g.* late endosomes or lysosomes), possibly contributing to the observed difference in their delivery-enhancing properties.[47] In line with this hypothesis, it was observed that under the given experimental conditions only ebastine induced a significant increase in total lysosomal volume, indicative of lysosomal swelling (Figure 1e). A notable change was also observed in the cell's side scatter (SSC) signal, which represents intracellular complexity and granularity and which was used before as a proxy for endolysosomal perturbation by CADs (Figure S1). Altogether, these data identify ebastine as a highly potent siRNA delivery enhancer in NSCLC cells, most likely via inducing lysosomal membrane damage, allowing siRNA leakage into the cytosol.

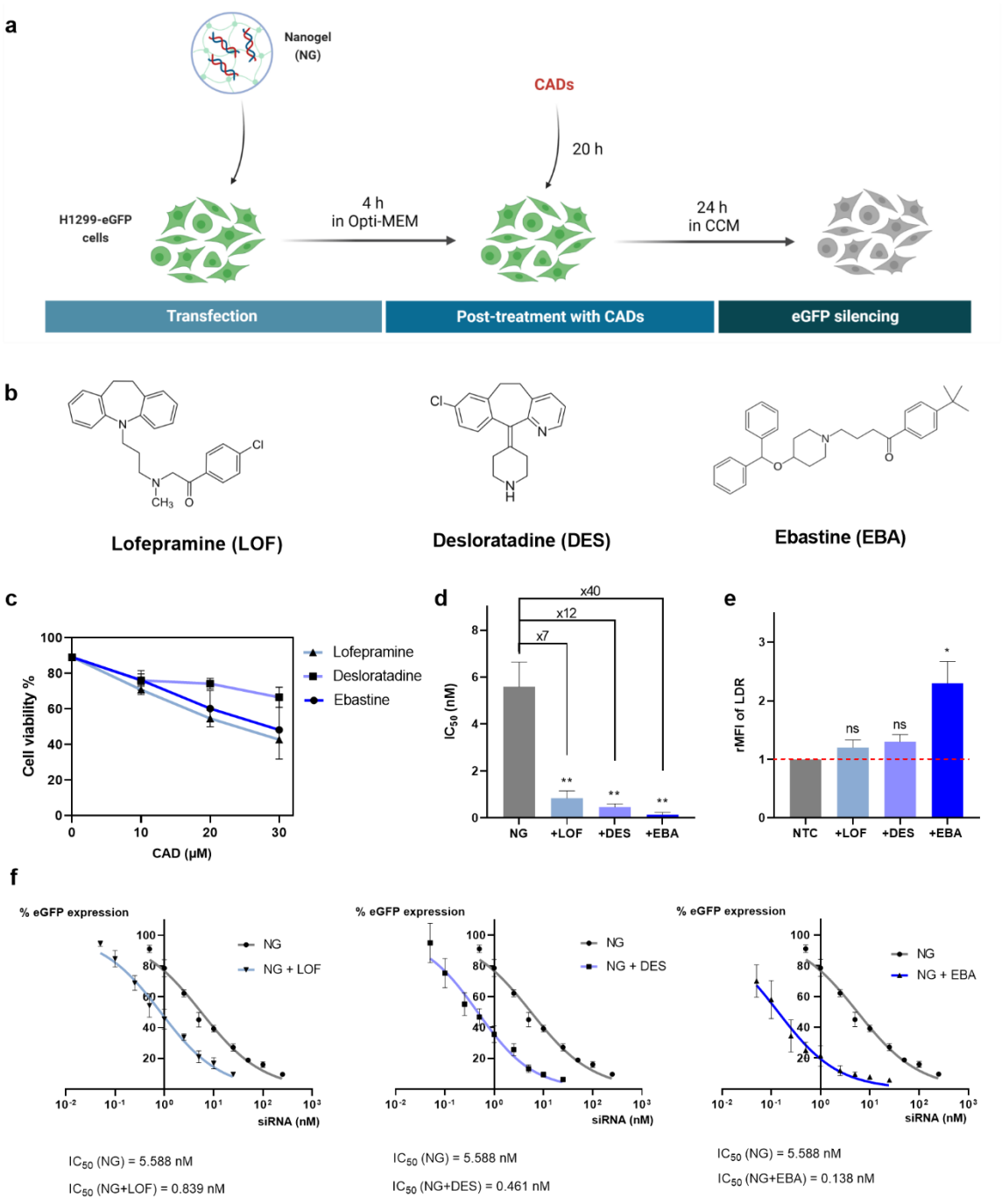

Figure 1. Impact of selected cationic amphiphilic drugs (CADs) on gene silencing efficiency of siRNA-loaded polysaccharide nanogels (NG) in H1299 cells. *(a) Schematic representation of experimental protocol. (b) Molecular structures of the three tested molecules (lofepramine, LOF; desloratadine, DES; ebastine, EBA). (c) Cell viability after treatment with NG and CAD molecules in a concentration range of 0-30 μM. (d, f) siRNA IC_{50} values (nM) and respective dose-response curves of the siRNA-induced eGFP silencing obtained with NG alone or post-treatment with CAD molecules (LOF 30 μM; DES 30 μM; EBA 15 μM). (e) Relative increase in*

*Lysotracker Deep Red (LDR) staining of H1299-eGFP cells as a function of CAD treatment. Data are presented as mean ± SEM (n=3). Statistical analysis was performed using One Way Anova with Tukey correction and significance is indicated as ns $p > 0.05$, * $p \leq 0.05$, ** $p \leq 0.01$. CADs = cationic amphiphilic drugs, CCM = complete cell culture medium, IC_{50} = half maximal inhibitory concentration, NTC = non treated cells.*

3.2 Ebastine improves cellular delivery of cholesterol-conjugated siRNA

Having identified ebastine as an siRNA delivery enhancer for polysaccharide NGs, we next sought to validate its effect on more clinically relevant delivery systems, including cholesterol-siRNA (chol-siRNA) conjugates (Figure 2a). It has been described that chol-siRNA can be effectively internalized by cells via endocytosis and induce significant knockdown.[48] However, the limited endosomal escape efficiency requires relatively high doses.[49] In line with these observations, incubating H1299-eGFP cells with chol-siRNA (50-500 nM) showed a concentration-dependent increase in cellular uptake (Figure 2b, c), albeit resulting in almost negligible eGFP silencing (Figure 2d). Exposing chol-siRNA transfected cells to ebastine (15 µM) substantially enhanced chol-siEGFP knockdown, leading to an additional 40-50% silencing (Figure 2d). Knockdown improvement could be extrapolated to other cell types, as demonstrated in an alternative lung cancer cell model (A549-eGFP cells) (Figure 2e). As was the case for the NG-transfected cells, this adjuvant effect coincided with strongly increased SSC and LDR signals, again suggesting the induction of lysosomal swelling (Figure 2f, g). These data corroborate earlier findings in which efficient chol-siRNA internalization followed by treatment with the CAD molecules siramesine and chloroquine induced chol-siRNA release from lysosomes.[47] Exposure of the cells to these compounds was also associated with a substantial increase in lysosomal size, which explained the observed increase in cytosolic siRNA delivery.[47] Taken together, our results suggest that ebastine can likewise be repurposed to improve cytosolic delivery of lipid-conjugated siRNAs.

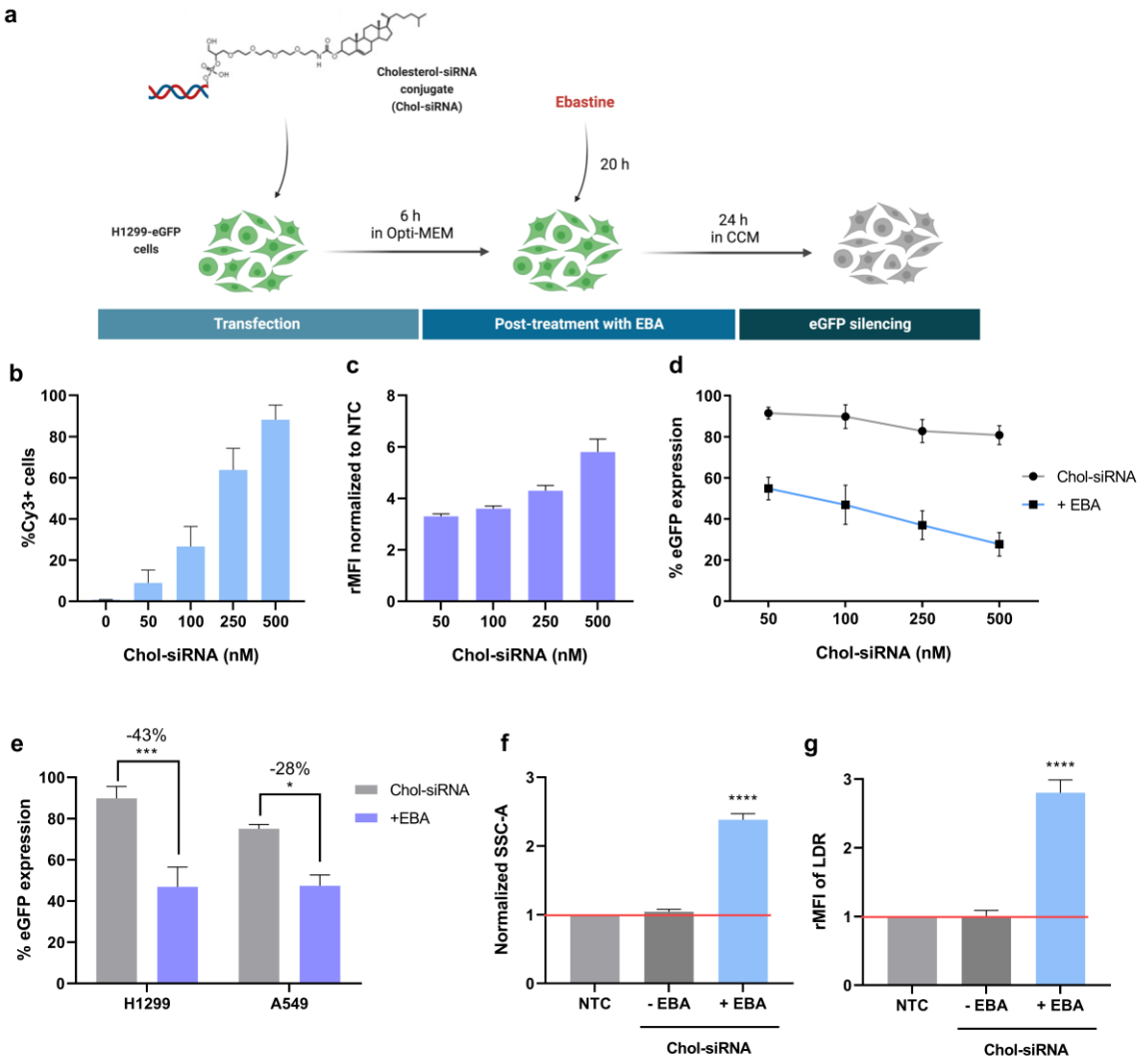

Figure 2. Adjuvant effect of ebastine on cholesterol-siRNA conjugates. *(a) Schematic representation of experimental workflow. (b) Percentage of H1299-eGFP cells that uptake Cy3-labeled chol-siRNA as a function of concentration (0 – 500 nM). (c) Relative mean fluorescence intensity (rMFI) increase in Cy3⁺ cells normalized to NTC. (d) Exposure of 50 – 500 nM chol-siEGFP transfected H1299-eGFP cells to 15 µM ebastine strongly promotes eGFP knockdown, as quantified by flow cytometry. (e) Comparison of ebastine-induced knockdown enhancement in two different lung cancer cell lines, H1299-eGFP and A549-eGFP, following transfection with 100 nM chol-siRNA. (f) Fold increase in side scatter (SSC) signal, normalized to NTC. (g) Fold increase in Lysotracker Deep Red (LDR) signal, expressed as rMFI, normalized to NTC. Data are presented as mean ± SEM (n=3). Chol-siRNA concentration in (e-g) is 100 nM. Statistical analysis was performed using One Way Anova with Tukey Correction and significance is*

*indicated as * $p \leq 0.05$, *** $p \leq 0.001$, **** $p \leq 0.0001$. CCM = complete cell culture medium, NTC = non treated cells, SSC-A = side scatter.*

3.3 Ebastine-mediated improvement of siRNA delivery via LNPs strongly depends on lipid composition

Next, we investigated the adjuvant potency of ebastine on a set of LNPs which varied in their type of ionizable lipid (DLin-MC3-DMA or CSL3) and PEGylation strategy (DMG-PEG_{2000} or DSPE-PEG_{2000}), using a comparable experimental workflow (Figure 3a, Figure S2a, S2b).[45,50] Physicochemical characterization of these LNP formulations, produced via microfluidic mixing, showed that MC3-LNPs have a smaller hydrodynamic diameter (~80 nm) compared to CSL3-LNPs (~130 nm), with all particles showing a PDI value below 0.3, which indicates acceptable polydispersity (Figure 3b). Cells were incubated with LNPs for a longer amount of time compared to chol-siRNA to account for a slower and delayed uptake kinetics of LNPs.[51] As expected, state-of-the-art LNPs mimicking the Onpattro formulation, *i.e.* containing the ionizable lipid DLin-MC3-DMA and DMG-PEG_{2000}, demonstrate excellent gene silencing efficiency (IC_{50} = 10 nM) (Figure 3e). However, substituting the DMG-PEG_{2000} with DSPE-PEG_{2000} completely abolishes the silencing effect (Figure 3c). As the physicochemical characteristics of both LNPs are equal, the latter result can most likely be explained by the so-called PEG dilemma.[52,53] PEG-lipids with shorter dialkyl chains (C14 for DMG-PEG) rapidly desorb from the LNP surface and are exchanged for apolipoprotein E (ApoE), thus allowing efficient endocytic uptake via the low-density lipoprotein (LDL) receptor.[17,54,55] In contrast, PEG-lipids with longer fatty acid tails (C18 for DSPE-PEG) remain stably anchored to the LNP. The stealth-like properties of such PEGylated LNPs might limit cellular interactions, leading to reduced cellular uptake and ineffective endosomal escape.[56] Independent of intrinsic LNP silencing efficiency, the addition of ebastine did not substantially improve knockdown efficiency, although a moderate decrease in IC_{50} was observed for the Onpattro formulation (IC_{50} = 7 nM) (Figure 3e). This result is largely in line with previously reported data by Van de Vyver *et al*., which suggested that the size of the CAD-induced pores in the limiting lysosomal membrane only allows diffusion of siRNA when released from its nanocarrier.[21] In a first step, the DLin-MC3-DMA ionizable lipid mediates LNP fusion with endolysosomal membranes by adopting an inverted hexagonal phase (H_{II}), responsible for the cytosolic release of 1-3% of

delivered siRNA.[17,57,58] Following this process, it is hypothesized that the residual siRNA-LNP complexes in the endolysosomal compartment remain tightly associated, thus precluding CAD-mediated endolysosomal escape. Following these insights, the adjuvant effect of ebastine was evaluated on LNPs constructed with a different pH-dependent switchable cationic ionizable lipid (CSL3) (Figure S2c). Upon protonation of the central pyridine in the endosomal compartment, the CSL3 lipid undergoes LNP-destabilizing conformational changes due to the formation of an intramolecular hydrogen bond, possibly facilitating release of the siRNA.[45] Interestingly, it was observed that ebastine strongly promoted knockdown efficiency of a previously reported optimal CSL3-LNP composition, despite the presence of 2.5 mol% of DSPE-PEG_{2000}. As it was demonstrated before that the lipid switching mechanism following the endosomal protonation of the CSL3 lipid was not affected by a stable PEG coating, these results support the abovementioned hypothesis (Figure 3d).[45]

On the other hand, substituting the 2.5 mol% DSPE-PEG_{2000} lipid in the CSL3-LNP with a conventional 1.5% DMG-PEG_{2000}, despite moderately improved LNP transfection efficiency, completely abolished its sensitivity to ebastine (Figure 3f). It remains to be investigated if PEG desorption and serum protein binding in the latter case could negatively impact the CSL3 lipid switching behavior (Figure S2c). Altogether, the data suggest that promoting intra-endosomal LNP destabilization could synergize with CAD exposure to promote cytosolic siRNA delivery from the lysosomal compartment. Previous research described that LNPs release their siRNA payload into the cytosol within a limited time span of ~10 minutes, mainly from $Rab5^+$ or $Rab7^+$ endocytic organelles.[16] Once trafficked towards $LAMP1^+$ compartments (*i.e.* lysosomes), no cytosolic siRNA release could be detected anymore.[16] As such, promoting siRNA release from endolysosomes with CADs such as ebastine could substantially improve the window of opportunity for cytosolic delivery. As unmodified siRNAs have been used in this work, which are more susceptible to enzymatic degradation in the endolysosomal compartment, it is hypothesized that cytosolic delivery can be even further promoted with chemically stabilized siRNAs.

a

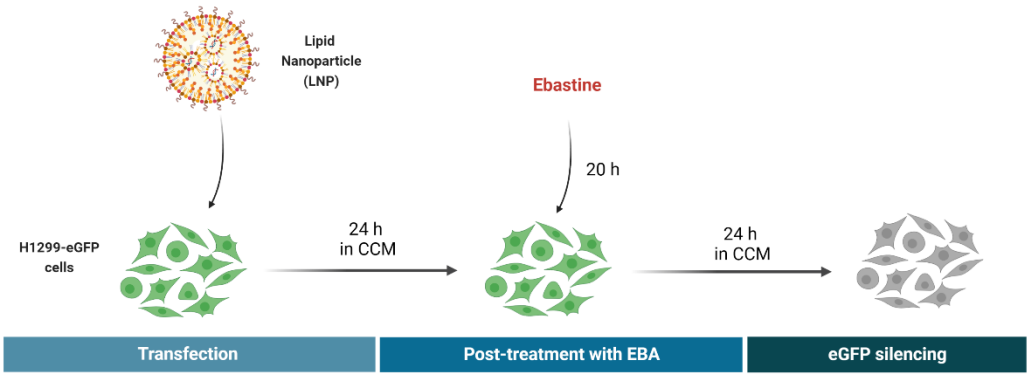

b

LNP	Size (nm)	PDI	EE %
MC3-DSPE	74.3 ± 1.5	0.243 ± 0.007	92.4 ± 1.3
CSL3-DSPE	135.6 ± 7.4	0.228 ± 0.022	89.7 ± 0.0
MC3-DMG	82.2 ± 1.3	0.285 ± 0.003	88.5 ± 0.2
CSL3-DMG	123.8 ± 1.6	0.209 ± 0.008	82.8 ± 0.3

c

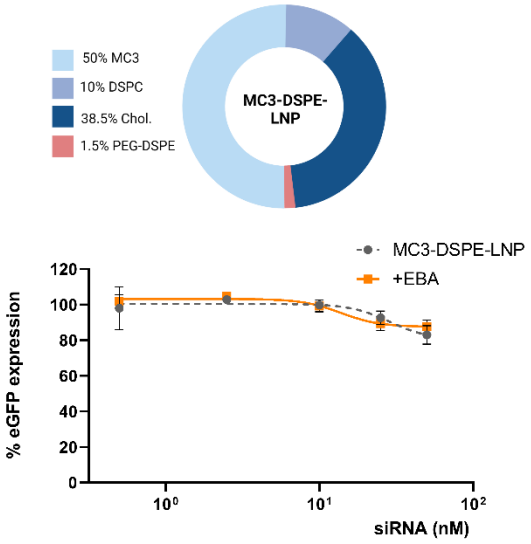

d

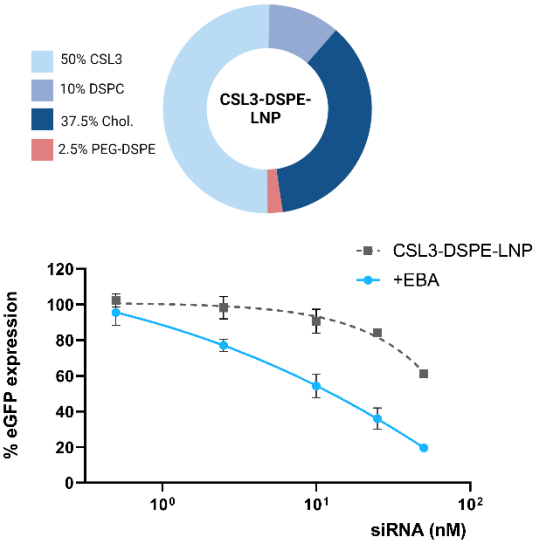

e

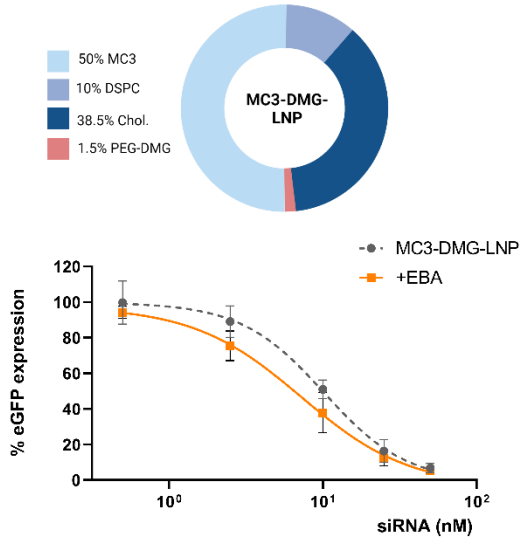

f

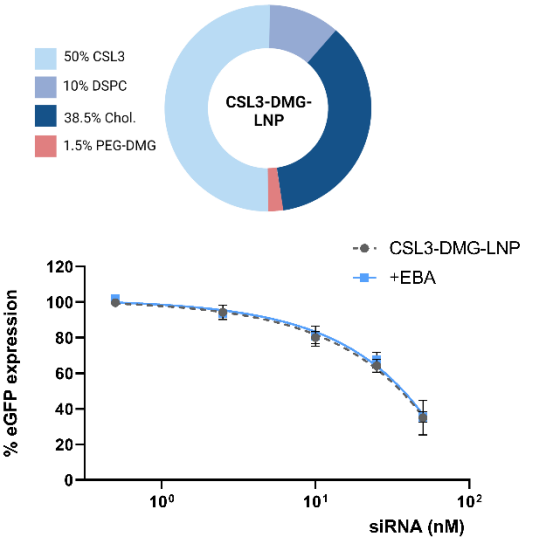

Figure 3. Adjuvant effect of ebastine on LNPs. *(a) Schematic representation of experimental workflow. (b) Physicochemical characterization of LNP's size and polydispersity index (PDI) by dynamic light scattering (DLS) and encapsulation efficiency values (EE %) ± standard deviation (technical triplicates). (c-f) Composition and transfection efficiencies of LNPs (0.5 – 50 nM) with and without the treatment with ebastine (15 µM). Transfection data are presented as mean ± SEM (n=3). CCM = complete cell culture medium, LNP = lipid nanoparticle.*

3.4 Induction of gene silencing by ebastine in a 3D tumor spheroid model

Finally, considering a higher additive effect of ebastine on chol-siRNA mediated knockdown and a more favorable penetration of this carrier in solid tissues, it was assessed if ebastine could improve gene silencing of chol-siRNA conjugates in a 3D tumor model of A549-eGFP cells (Figure 4a). In contrast to 2D cell culture monolayers, tumor spheroids represent a more relevant model mimicking the *in vivo* solid tumor tissue since it can reproduce differential penetration of oxygen, nutrients and drugs from the periphery to the inner core.[39,59] At first, we verified the toxicity of ebastine on 3D spheroids (530 ± 30 µm) after 20 h incubation with the compound. Only about 30% of cells in the tumor spheroids remained viable when exposed to the highest ebastine concentration (Figure 4b, c). Moreover, when exposed to mounting ebastine concentrations, (most likely dying) cells are released from the main spheroid body (Figure S3). As anticipated based on its physicochemical properties, this observation suggests a relatively easy access of ebastine to the deeper cell layers. Likewise, we verified if the chol-siRNA conjugate could penetrate the tumor spheroids. After applying Cy3-labeled chol-siRNA (1 µM), cellular uptake was quantified by flow cytometry on dissociated spheroids. Here, almost 80% of tumor cells had acquired the fluorescently-labeled chol-siRNA and displayed a 6-fold higher fluorescence compared to non-treated cells (Figure 4d, e). Confocal microscopy images at 50 µm depth likewise showed a dispersed Cy3 signal, confirming spheroid penetration of the chol-siRNA (Figure 4f). These results are in line with previous reports of chol-siRNA diffusion towards the core of cancer cell-derived spheroids.[47]

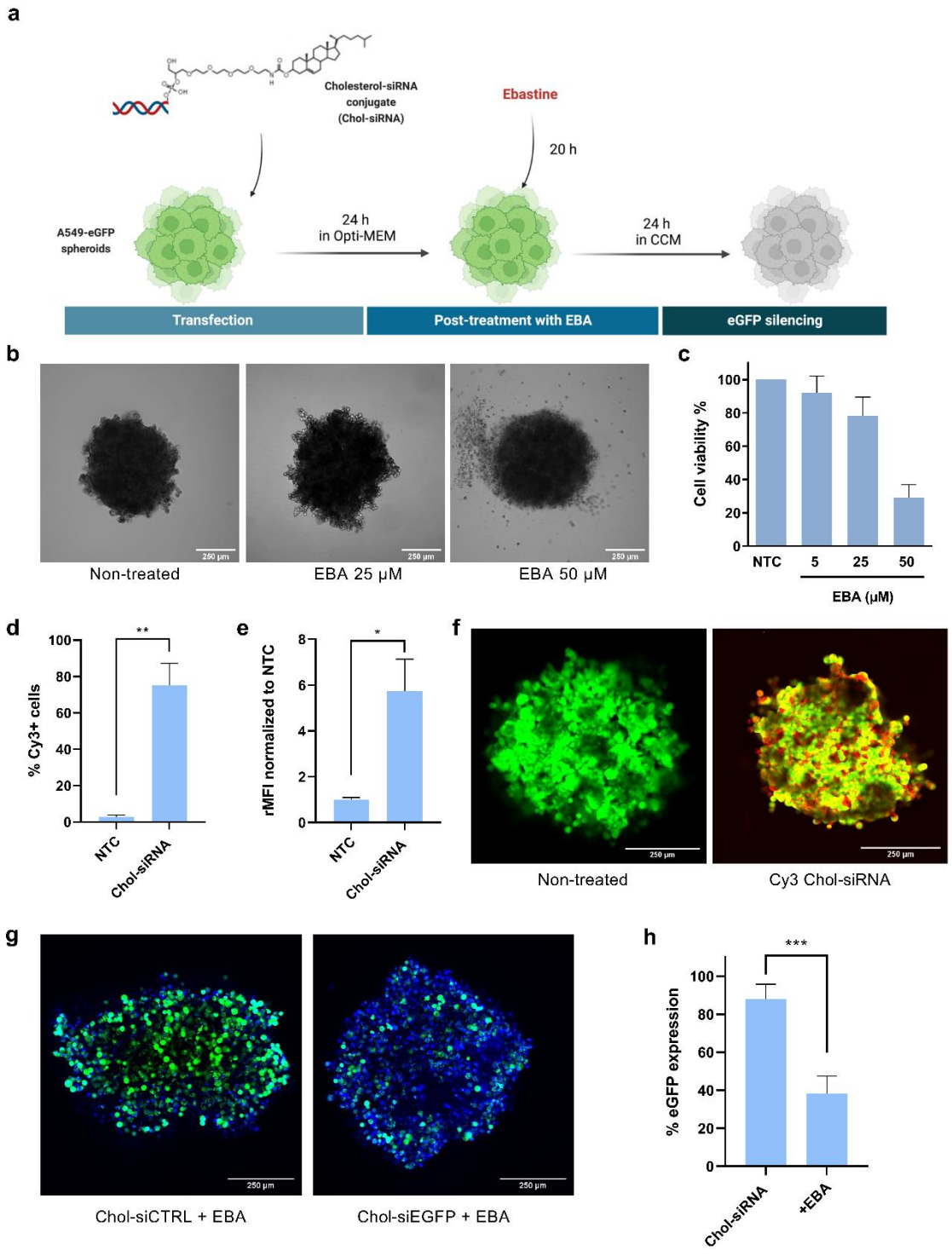

Figure 4. Ebastine-promoted silencing efficiency of chol-siRNA in a tumor spheroid model. (a) Schematic representation of experimental layout. (b) Transmission microscopy images of ebastine-induced cytotoxicity on A549-eGFP spheroids. (c) Cell viability following a 20 h treatment with ebastine (0-50 µM). (d-e) Percentage of positive cells and relative mean fluorescence intensity (rMFI) of cells that acquired Cy3-labeled chol-siRNA (1 µM) normalized

*towards non-treated cells (NTC). (f) Confocal microscopy images of Cy3-labeled chol-siRNA (1 µM) penetration in the spheroid (~530 µm diameter). (g) Confocal microscopy of eGFP silencing in spheroids transfected with chol-siCTRL and chol-siEGFP (400 nM), both treated with ebastine (35 µM). (h) Flow cytometric quantification of eGFP silencing achieved with addition of ebastine (35 µM) following transfection with 400 nM chol-siEGFP normalized towards chol-siCTRL. Cell viability data are presented as mean ± SEM (n=3). Cy3 chol-siRNA uptake and eGFP silencing are presented as mean ± SEM of three spheroids. Statistical analysis was performed using student t-test for direct comparison of two conditions and significance is indicated as * p ≤ 0.05, ** p ≤ 0.01, *** p ≤ 0.001. CCM = complete cell culture medium.*

Having ensured that both the chol-siRNA conjugate and the ebastine can diffuse into the tumor spheroid, the impact of ebastine on chol-siRNA induced gene silencing was subsequently tested (Figure 4a). Hereto, we applied an EBA concentration of 35 µM, maintaining ~50% cell viability (Figure 4c). Both confocal microscopy on intact spheroids and flow cytometry following spheroid dissociation showed a marked decrease in eGFP expression with ebastine treatment, i.e. from 85% to 38% (Figure 4g, h). Hence, the ebastine-induced knockdown enhancement in tumor spheroids confirms earlier results obtained on 2D cell cultures. These results are encouraging towards *in vivo* translation and provide opportunities for combining oncogene-targeting chol-siRNA conjugates and antihistamine CADs such as ebastine, *e.g.* through local intratumoral injection. Moreover, as it is known that chol-siRNA conjugates accumulate in lysosomal compartments, multiple rounds of adjuvant exposure could induce multiple lysosomal escape events, as demonstrated before for polysaccharide NGs.[20,47] It will be interesting to see if this adjuvant strategy could be extrapolated to other types of siRNA conjugates as well, including other lipid-modified siRNAs.

4. Conclusion

Therapeutic application of RNA-based drugs is still hindered by inefficient cytosolic delivery. Cationic amphiphilic drugs (CADs) are widely-used drugs which, due to their particular physicochemical properties, can diffuse through cellular membranes and accumulate in acidified lysosomes. Here, they induce lysosomal swelling and transient lysosomal membrane permeabilization (LMP), allowing siRNA molecules to escape from the lysosome into the cytosol. In this work, we identified the antihistamine CAD ebastine as a highly potent siRNA delivery enhancer in a non-small cell lung cancer cell model, leading to a 40-fold improved silencing efficiency of a cationic hydrogel nanocarrier. Moreover, ebastine likewise promoted gene knockdown by both cholesterol-conjugated siRNAs (chol-siRNAs) as well as lipid nanoparticles (LNPs), demonstrating the versatility of the compound and its compatibility with state-of-the-art siRNA delivery strategies. Interestingly, the effect of ebastine was strongly dependent on LNP composition, only showing improved gene knockdown for a pH-dependent switchable ionizable lipid and when a stable PEGylation strategy was applied. Gene knockdown enhancement of chol-siRNAs obtained on a monolayer cell culture could be replicated in a 3D tumor spheroid model. Overall, we believe that the repurposing of ebastine as an siRNA delivery-promoting agent could be a promising drug combination strategy in cancer treatment.

Acknowledgments

The authors acknowledge the Ghent Light Microscopy Core (GLiM) for use of microscopy facilities and training. K.R. and C.M. acknowledge the Research Foundation Flanders (FWO) for funding through research grant G039419N. K.R. additionally acknowledges the European Research Council (ERC) for funding received under the European Union's Horizon 2020 research and innovation program (Grant agreement No. 101002571).

References

1. Fire, A. *et al.* Potent and specific genetic interferenceby double-strandedRNA in Caenorhabditiselegans Andrew. *Nature* **391,** 806–811 (1998).

2. Dammes, N. & Peer, D. Paving the Road for RNA Therapeutics. *Trends Pharmacol. Sci.* **41,** 755–775 (2020).

3. Micklefield, J. Backbone Modification of Nucleic Acids: Synthesis, Structure and Therapeutic Applications. *Curr. Med. Chem.* **8,** 1157–1179 (2012).

4. Sun, Y. *et al.* Enhancing the therapeutic delivery of oligonucleotides by chemical modification and nanoparticle encapsulation. *Molecules* **22,** (2017).

5. Kanasty, R., Dorkin, J. R., Vegas, A. & Anderson, D. Delivery materials for siRNA therapeutics. *Nat. Mater.* **12,** 967–977 (2013).

6. Akinc, A. *et al.* The Onpattro story and the clinical translation of nanomedicines containing nucleic acid-based drugs. *Nat. Nanotechnol.* **14,** 1084–1087 (2019).

7. Foster, D. J. *et al.* Advanced siRNA Designs Further Improve In Vivo Performance of GalNAc-siRNA Conjugates. *Mol. Ther.* **26,** 708–717 (2018).

8. Janas, M. M. *et al.* Safety evaluation of 2-deoxy-2-fluoro nucleotides in GalNAc-siRNA conjugates. *Nucleic Acids Res.* **47,** 3306–3320 (2019).

9. Zhang, M. M., Bahal, R., Rasmussen, T. P., Manautou, J. E. & Zhong, X. bo. The growth of siRNA-based therapeutics: Updated clinical studies. *Biochem. Pharmacol.* **189,** (2021).

10. Ly, S. *et al.* Visualization of self-delivering hydrophobically modified siRNA cellular internalization. *Nucleic Acids Res.* **45,** 15–25 (2017).

11. Osborn, M. F. & Coles, A. H. Efficient gene silencing in brain tumors with hydrophobically modified siRNAs. *Cogn. Emot. J.* **30,** 1289–1303 (2016).

12. Chernikov, I. V. *et al.* Cholesterol-Containing Nuclease-Resistant siRNA Accumulates in Tumors in a Carrier-free Mode and Silences MDR1 Gene. *Mol. Ther. - Nucleic Acids* **6,** 209–220 (2017).

13. Van de Vyver, T., De Smedt, S. C. & Raemdonck, K. Modulating intracellular pathways to improve non-viral delivery of RNA therapeutics. *Adv. Drug Deliv. Rev.* **181,** 114041 (2022).

14. Joris, F., De Smedt, S. C. & Raemdonck, K. Small molecules convey big messages: Boosting non-viral nucleic acid delivery with low molecular weight drugs. *Nano Today* **16,** 14–29 (2017).

15. Smith, S. A., Selby, L. I., Johnston, A. P. R. & Such, G. K. The Endosomal Escape of Nanoparticles: Toward More Efficient Cellular Delivery. *Bioconjug. Chem.* **30,** 263–272 (2019).

16. Wittrup, A. *et al.* Visualizing lipid-formulated siRNA release from endosomes and target gene knockdown. **344,** 1173–1178 (2015).

17. Gilleron, J. *et al.* Image-based analysis of lipid nanoparticle-mediated siRNA delivery, intracellular trafficking and endosomal escape. *Nat. Biotechnol.* **31,** 638–646 (2013).

18. Brown, C. R. *et al.* Investigating the pharmacodynamic durability of GalNAc-siRNA conjugates. *Nucleic Acids Res.* **48,** 11827–11844 (2021).

19. Dowdy, S. F. Overcoming cellular barriers for RNA therapeutics. *Nat. Biotechnol.* **35,** 222–229 (2017).

20. Joris, F. *et al.* Repurposing cationic amphiphilic drugs as adjuvants to induce lysosomal siRNA escape in nanogel transfected cells. *J. Control. Release* **269,** 266–276 (2018).

21. Van de Vyver, T. *et al.* Cationic Amphiphilic Drugs Boost the Lysosomal Escape of Small Nucleic Acid Therapeutics in a Nanocarrier-Dependent Manner. *ACS Nano* **14,** 4774–4791 (2020).

22. Lemieux, B., Percival, M. D. & Falgueyret, J. P. Quantitation of the lysosomotropic character of cationic amphiphilic drugs using the fluorescent basic amine Red DND-99. *Anal. Biochem.* **327,** 247–251 (2004).

23. Kallunki, T., Olsen, O. D. & Jäättelä, M. Cancer-associated lysosomal changes: Friends or foes? *Oncogene* **32,** 1995–2004 (2013).

24. Bogaert, B. *et al.* A lipid nanoparticle platform for mRNA delivery through repurposing of cationic amphiphilic drugs. *J. Control. Release* **350,** 256–270 (2022).

25. Gavini, J. *et al.* Verteporfin-induced lysosomal compartment dysregulation potentiates the effect of sorafenib in hepatocellular carcinoma. *Cell Death Dis.* **10,** (2019).

26. Garcia, E. A., Bhatti, I., Henson, E. S. & Gibson, S. B. Prostate Cancer Cells Are Sensitive to Lysosomotropic Agent Siramesine through Generation Reactive Oxygen Species and in Combination with Tyrosine Kinase Inhibitors. *Cancers (Basel).* **14,** 5478 (2022).

27. Jaffrézou, J. P. *et al.* Inhibition of lysosomal acid sphingomyelinase by agents which reverse multidrug resistance. *BBA - Mol. Cell Res.* **1266,** 1–8 (1995).

28. Pagliero, R. J. *et al.* Discovery of Small Molecules That Induce Lysosomal Cell Death in Cancer Cell Lines Using an Image-Based Screening Platform. *Assay Drug Dev. Technol.* **14,** 489–510 (2016).

29. Petersen, N. H. T. *et al.* Transformation-Associated Changes in Sphingolipid Metabolism Sensitize Cells to Lysosomal Cell Death Induced by Inhibitors of Acid Sphingomyelinase. *Cancer Cell* **24,** 379–393 (2013).

30. Ellegaard, A. M. *et al.* Repurposing Cationic Amphiphilic Antihistamines for Cancer Treatment. *EBioMedicine* **9,** 130–139 (2016).

31. Roberts, D. J. A Preclinical Overview of Ebastine. *Drugs* **52,** 8–14 (1996).

32. Anand, A. *et al.* Cell death induced by cationic amphiphilic drugs depends on lysosomal Ca2+ release and cyclic AMP. *Mol. Cancer Ther.* **18,** 1602–1614 (2019).

33. Cornet-Masana, J. M. *et al.* Dual lysosomal-mitochondrial targeting by antihistamines to eradicate leukaemic cells. *EBioMedicine* **47,** 221–234 (2019).

34. Verdoodt, F. *et al.* Antihistamines and ovarian cancer survival: Nationwide cohort study and in vitro cell viability assay. *J. Natl. Cancer Inst.* **112,** 964–967 (2020).

35. Berkeley, L. Killing from the inside. 2–3 (2013).

36. Gulbins, E. & Kolesnick, R. N. It Takes a CAD to Kill a Tumor Cell with a LMP. *Cancer Cell* **24,** 279–281 (2013).

37. Li, H. *et al.* The allergy mediator histamine confers resistance to immunotherapy in cancer patients via activation of the macrophage histamine receptor H1. *Cancer Cell* **40,** 36–52.e9 (2022).

38. Chiang, C. H. *et al.* Efficacy of cationic amphiphilic antihistamines on outcomes of patients treated with immune checkpoint inhibitors. *Eur. J. Cancer* **174,** 1–9 (2022).

39. Peirsman, A. *et al.* MISpheroID: a knowledgebase and transparency tool for minimum information in spheroid identity. *Nat. Methods* **18,** 1294–1303 (2021).

40. Raemdonck, K. *et al.* Biodegradable dextran nanogels for RNA interference: Focusing on endosomal escape and intracellular siRNA delivery. *Adv. Funct. Mater.* **19,** 1406–1415 (2009).

41. Raemdonck, K., Naeye, B., Høgset, A., Demeester, J. & De Smedt, S. C. Prolonged gene silencing by combining siRNA nanogels and photochemical internalization. *J. Control. Release* **145,** 281–288 (2010).

42. De Backer, L. *et al.* Bio-inspired pulmonary surfactant-modified nanogels: A promising siRNA delivery system. *J. Control. Release* **206,** 177–186 (2015).

43. Merckx, P. *et al.* Surfactant protein B (SP-B) enhances the cellular siRNA delivery of proteolipid coated nanogels for inhalation therapy. *Acta Biomater.* **78,** 236–246 (2018).

44. Raemdonck, K., Naeye, B., Høgset, A., Demeester, J. & De Smedt, S. C. Prolonged gene silencing by combining siRNA nanogels and photochemical internalization. *J. Control. Release* **145,** 281–288 (2010).

45. Viricel, W. *et al.* Cationic switchable lipids: pH-triggered molecular switch for siRNA delivery. *Nanoscale* **9,** 31–36 (2017).

46. Schindelin, J. *et al.* Fiji: an open-source platform for biological-image analysis. *Nat. Methods* **9,** 676–682 (2012).

47. Du Rietz, H., Hedlund, H., Wilhelmson, S., Nordenfelt, P. & Wittrup, A. Imaging small molecule-induced endosomal escape of siRNA. *Nat. Commun.* **11,** (2020).

48. Wolfrum, C. *et al.* Mechanisms and optimization of in vivo delivery of lipophilic siRNAs. *Nat. Biotechnol.* **25,** 1149–1157 (2007).

49. Zheng, Y. & Tai, W. Insight into the siRNA transmembrane delivery—From cholesterol conjugating to tagging. *Wiley Interdiscip. Rev. Nanomedicine Nanobiotechnology* **12,** 1–10 (2020).

50. Zhang, Y., Sun, C., Wang, C., Jankovic, K. E. & Dong, Y. Lipids and Lipid Derivatives for RNA Delivery. *Chem. Rev.* (2021). doi:10.1021/acs.chemrev.1c00244

51. Gilleron, J. *et al.* Identification of siRNA delivery enhancers by a chemical library screen. *Nucleic Acids Res.* **43,** 7984–8001 (2015).

52. Zalba, S., ten Hagen, T. L. M., Burgui, C. & Garrido, M. J. Stealth nanoparticles in oncology: Facing the PEG dilemma. *J. Control. Release* **351,** 22–36 (2022).

53. Hatakeyama, H., Akita, H. & Harashima, H. The polyethyleneglycol dilemma: Advantage and disadvantage of PEGylation of liposomes for systemic genes and nucleic acids delivery to tumors. *Biol. Pharm. Bull.* **36,** 892–899 (2013).

54. Akinc, A. *et al.* The Onpattro story and the clinical translation of nanomedicines containing nucleic acid-based drugs. *Nat. Nanotechnol.* **14,** (2019).

55. Akinc, A. *et al.* Targeted delivery of RNAi therapeutics with endogenous and exogenous ligand-based mechanisms. *Mol. Ther.* **18,** 1357–1364 (2010).

56. Hald, C. *et al.* The role of lipid components in lipid nanoparticles for vaccines and gene therapy. *Adv. Drug Deliv. Rev.* **188,** 114416 (2022).

57. Schlich, M. *et al.* Cytosolic delivery of nucleic acids: The case of ionizable lipid nanoparticles. *Bioeng. Transl. Med.* **6,** 1–16 (2021).

58. Ferraresso, F. *et al.* Comparison of DLin-MC3-DMA and ALC-0315 for siRNA Delivery to Hepatocytes and Hepatic Stellate Cells. *Mol. Pharm.* **19,** 2175–2182 (2022).

59. Johnston, S. S. P. A. The Production of 3D Tumor Spheroids for Cancer Drug Discovery. *Physiol. Behav.* **176,** 100–106 (2016).